Exploiting Flexibility of Integrated Demand Response to Alleviate Power Flow Violation During Line Tripping Contingency

Tong Cheng, *Student Member*, *IEEE*, Zhenfei Tan, *Student Member*, *IEEE*, and Haiwang Zhong, *Senior Member*, *IEEE*

***Abstract*—Multi-energy integrations provide great opportunities for economic and efficient resource utilization. In the meantime, power system operation requires enough flexible resources to deal with contingencies such as transmission line tripping. Besides economic benefits, this paper focuses on the security benefits that can be provided by multi-energy integrations. This paper first proposes an operation scheme to coordinate multiple energy production and local system consumption considering transmission networks. The integrated flexibility model, constructed by the feasible region of integrated demand response (IDR), is then formulated to aggregate and describe local flexibility. Combined with system security constraints, a multi-energy system operation model is formulated to schedule multiple energy production, transmission, and consumption. The effects of local system flexibility on alleviating power flow violations during $N-1$ line tripping contingencies are then analyzed through a multi-energy system case. The results show that local system flexibility can not only reduce the system operation costs, but also reduce the probability of power flow congestion or violations by approximately 68.8% during $N-1$ line tripping contingencies.**

***Index Terms*—Multi-energy system, integrated flexibility, feasible region, integrated demand response, $N-1$ security.**

NOMENCLATURE

A. Indices and Sets

$\mathcal{N}^P$	Set of power system nodes
$\mathcal{N}^G$	Set of gas system nodes
$\mathcal{N}^H$	Set of heat system nodes
$\mathcal{N}_m^{gn}$	Set of gas nodes connected with gas node m
$\mathcal{T}$	Set of time intervals
$\mathcal{U}^G$	Set of generators
$\mathcal{U}^{CF}$	Set of coal-fired generators
$\mathcal{U}^{GF}$	Set of gas-fired generators
$\mathcal{U}^{CHP}$	Set of combined heat and power units
$\mathcal{U}^{GB}$	Set of gas boilers
$\mathcal{U}^{gc}$	Set of gas compressors
$\mathcal{U}_m^{gc}$	Set of gas compressors at gas node m
$\mathcal{U}^{gl}$	Set of contracted gas loads
$\mathcal{U}_m^{gl}$	Set of gas loads at gas node m
$\mathcal{U}^{gs}$	Set of gas suppliers
$\mathcal{U}_m^{gs}$	Set of gas suppliers at gas node m
$\mathcal{L}^P$	Set of power transmission lines
$\mathcal{L}^H$	Set of pipes in heat networks
$\mathcal{L}_q^{H,+}$, $\mathcal{L}_q^{H,-}$	Set of pipes with fluid flowing into and out of node q
$\mathcal{L}^{H,s/b}$	Set of pipes in heat supply/return networks
$\mathcal{L}^{Hs/Hl}$	Set of pipes connected with heat source/load
$\mathcal{L}_q^H$	Set of pipes connected with node q
g	Index for generator units
i	Index for units
j	Index for gas compressors
k	Index for power transmission lines
l	Index for gas loads
m, n, q	Index for nodes
p	Index for heat pipes
s	Index for gas suppliers
t	Index for time intervals

B. Parameters and Constants

λ	Heat conduction coefficient
σ	A fixed penalty factor
ρ_i	Gas contract price for gas consumer i
$\pi_{m,\max}$, $\pi_{m,\min}$	The maximum and minimum pressures at gas node m
a_j, b_j, c_j	Gas consumption-related constants of compressor j
c	Specific heat of the fluid

Manuscript received: August 3, 2021; revised: November 13, 2021; accepted: January 25, 2022. Date of CrossCheck: January 25, 2022. Date of online publication: February 22, 2022.

This work was supported by State Grid Corporation of China "Research on Multi-energy System Energy Conversion Simulation and Energy Efficiency Evaluation" (No. SGTYHT/18-JS-206).

T. Cheng, Z. Tan, and H. Zhong (corresponding author) are with the State Key Laboratory of Power Systems, the Department of Electrical Engineering, Tsinghua University, Beijing, China (e-mail: ct20@mails.tsinghua.edu.cn; zftan@outlook.com; zhonghw@tsinghua.edu.cn).

DOI: 10.35833/MPCE.2021.000535

C_i^{boiler} Gas-heat conversion coefficient of boiler i

C_i^{CHP} Heat-power ratio of combined heat and power (CHP) unit i

C_{mn} Gas pipeline constant from node m to n

$F_{k,\max}$ Capacity of transmission line k

$GSDF_{k,n}$ Generation shift distribution factor of node n to line k

$H_{j,\max}$, $H_{j,\min}$ The maximum and minimum horsepower of gas compressor j

k_{j1}, k_{j2}, α Gas flow-related constants of compressor j

L_p Length of pipe p

m_p Fluid flow of pipe p

$N(g)$ Node of generator g

$P_{g,\max}$, $P_{g,\min}$ The maximum and minimum capacities of generator g

$Ramp_g$ Ramp rate of generator g

SR_t^r Required spinning reserve of the system at time t

$t_{g,\min}^{off}$ The minimum shutdown time of generator g

$t_{g,\min}^{on}$ The minimum start-up time of generator g

$T_{\max}^{s/b}$, $T_{\min}^{s/b}$ The maximum and minimum temperatures of fluid supply/return pipe

T_a Environment temperature

$v_{s,\max}$, $v_{s,\min}$ The maximum and minimum gas injections of gas supplier s

C. Variables

π_m Gas pressure of node m

f_{mn} Gas flow from gas node m to n

$F_{f,j}$ Gas consumption of compressor j

H_j Power of gas compressor j

$L_{i,t}$ Flow of the gas input of unit i at time t

L_l Flow of gas load l

$P_{g,t}$ Power output of generator g at time t

$P_{k,t}$ Power transmission of line k at time t

$P_{n,t}^L$ Power load of node n at time t

$Q_q^{s/l}$ Heat supply/load of node q

$Q_{i,t}$ Heat output of unit i at time t

sl_k Slack variables introduced for line k

$SU_{i,t}$, $SD_{i,t}$ Start-up and shut-down costs of unit i at time t

$T_{p,in}^{s/b}$ Temperature of inflow of supply/return pipe p

$T_{p,out}^{s/b}$ Temperature of outflow of supply/return pipe p

$T_q^{s/b}$ Temperature of the outflow of node q in the supply/return system

$U_{g,t}$ Working status of generator g at time t

v_s Flow of gas supply s

$W_{i,t}$ Gas cost of unit i at time t

$Y_{g,t}$ Start-up status of generator g at time t

$Z_{g,t}$ Shut-down status of generator g at time t

I. Introduction

WITH the concept of carbon-free energy system transition, multi-energy systems have gained much attention due to their superiority in utilizing complementary energy resources and improving energy efficiency.

Large-scale interconnected energy systems provide great opportunities for economic and efficient resource utilization in a larger spatial range. In the on-going practice of multi-energy integrations, different energy carriers are coupled and integrated in various sectors of the entire energy supply chain, from energy production, transmission/transportation, to distribution and consumption. Multi-energy carriers interact with each other at various spatial levels, from regional systems (e.g., urban energy supply infrastructure) downscaling to local systems (e.g., smart buildings, energy communities, and industrial parks). These interactions not only provide chances for system operators to maximize social welfare but also play an important role in enhancing the resilience and stability of the whole system.

More specifically, the flexibility provided by multi-energy integrations may help any single system handle contingency situations. Taking the power system as an example, the flexibility may help to avoid power flow violations and thus reduce transmission line investment, which will be further discussed in this paper. Actually, security is always a key requirement of power system operation [1]. The security-constrained unit commitment (SCUC) problem, which considers both the normal states and the $N-1$ contingency states, is commonly used to decide the short-term schedule of power systems.

The power system unit commitment problem considering $N-1$ contingencies can be divided into two categories: preventive control and corrective control. For both categories, the system operator considers all possible $N-1$ conditions and derives a day-ahead schedule result. The difference lies in the fact that the preventive control requires the system to operate safely without changing the schedule of generators, while the corrective control allows generators to change their output to relieve the power flow violation in a given time.

Reference [2] proposes a DC optimal power flow (DCOPF) based preventive SCUC model with $N-1$ reliability, in which all contingency conditions are embedded into the optimization problem through integer variables. Furthermore, a line outage distribution factor-based method is proposed in [3] to reduce the computational burden of the problem. However, as stated in [4], the preventive control does not consider the real-time adjustment ability of generators, thus making the dispatch order too conservative and compromising the economic efficiency of the system. A DCOPF-based corrective SCUC model considering the long-term emergency (LTE) and short-term emergency (STE) rates is then proposed. The application of the so-called LTE/STE allows the temporal exceedance of transmission capacity in post-contingency operation to make the system schedule less conservative according to [5]. An AC contingency dispatch model based on preventive/corrective control is proposed in [6] to balance the system economic and security properties.

However, few studies realize the potential of demand-side adjustment on $N-1$ reliability, which may lead to unnecessary investment in new transmission lines. Demand response programs have long been used to enhance system economic and security performance such as to maximize social welfare [7] and avoid voltage collapse [8]. With multi-energy interaction, conventional demand response programs can also turn into integrated demand response (IDR) programs [9]. In this way, the demand side can also change its load composition to adjust the line flow taking advantage of the flexibility of other systems. For example, the local system can use more heat instead of electricity to alleviate congestion in power transmission lines.

In fact, the IDR has been widely studied in recent years. IDR programs can be utilized to inhibit demand, adjust load curves, and improve customer satisfaction through different price signals and operation strategies [10]. An incentive-based IDR program and its model are proposed in [11] to reduce the total cost of the multi-energy aggregator. In [12], a price-based IDR scheme is proposed for integrated electricity and natural gas systems to demonstrate its potential of switching energy resources to maximize profits and a potential game model is proposed. In [13], a demand response program of smart buildings in integrated heat and electricity system is studied to provide heat and electricity balancing power. A production scheduling model for manufacturers considering electricity and gas demand response is established in [14] to save energy costs. In [15], an IDR optimization model that considers network constraints is proposed.

Despite the research progress in IDR models such as price-based, game theory-based, and smart energy hub (SEH) models and the coordinated optimization scheme of IDR with networks, few studies focus on and quantify the impact of IDRs on the system security margin. In [16], an $N-1$ security-constrained scheduling model for integrated electricity and gas systems is proposed, through which the influence of electricity transmission lines and gas pipeline tripping on the integrated system is further discussed. In [17], the static security influence of the exit of coupling elements in integrated energy systems is analyzed. However, the potential of integrated flexibility in dealing with contingencies is not considered.

In mainstream IDR research, IDR usually operates in a certain status according to given price signals, certain incentives or a game model. However, to perform quantitative research on the impact of IDR on the system security level, the feasible region of the local integrated energy should be determined and then combined with the network constraints to form a coordinated optimization problem. The feasible region of IDR, called the integrated flexibility region, can be established based on our previous work [18] to quantify the flexibility provided by the local IDR. Then, we apply a corrective $N-1$ contingency model and loosen the line capacity constraints. By introducing slack variables to these constraints, the benefits of the flexibility of IDRs in alleviating violations are further reflected.

The main contributions of this paper include the following two aspects.

1) A coordination scheme is proposed to utilize the flexibility of multi-energy conversion to alleviate power system $N-1$ contingency violations.

2) An explicit model is formulated to characterize the feasible region of the IDR, which can be embedded into the power system $N-1$ schedule problem without specific local system information, and thus the effect of the flexibility of IDR is analyzed.

The rest of this paper is organized as follows. In Section II, the system framework, including its structure and coordination scheme, is stated. In Section III, the specific mathematical model, including feasible region model of IDR and network model, is formulated. In Section IV, the performance of the proposed framework is demonstrated through a multi-energy case system. Conclusions are drawn in Section V.

II. System Framework

A. System Structure

A conceptual framework of the regional and local multi-energy systems is illustrated in Fig. 1. The regional multi-energy system consists of multiple energy resources, energy converters, and energy networks. In this study, the energy resources are the only interface through which the regional multi-energy system imports energy from external systems. Energy resources include, for instance, natural gas input, electricity from the external grid, and fossil fuels to drive generators. The overall operation costs of the entire system are only associated with the price and consumed amount of energy resources. Energy converters enable the integration of multi-energy flows by converting a single kind of energy input to other kinds of energy outputs. In the existing regulation framework, the networks connecting energy resources, converters, and loads are usually monopolized by a utility for a certain region. The regional system operator (RSO) optimally schedules the energy converters to supply the multi-energy demand (MED) of consumers with the minimum operation cost.

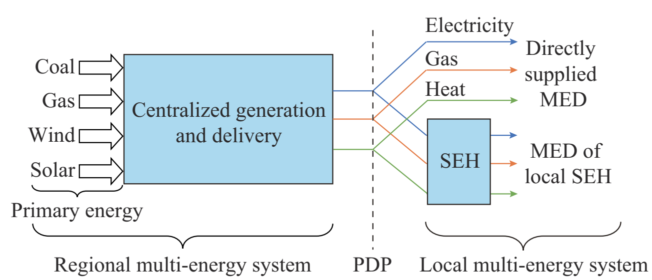

Fig. 1. Conceptual framework of regional and local multi-energy systems.

The energy consumers connected to the regional system can be classified into two types, namely the directly supplied MED and MED of local SEH. The former is directly connected to a node of the regional system, and its demand turns out to be the fixed boundary condition in utility-level regional system scheduling. The latter is equipped with local energy converters, which convert the energy supplied by the regional system to serve the terminal MED. With energy converters, the local multi-energy system is endowed with the ability to adjust its energy inputs without affecting the terminal MED, which provides operation flexibility to the regional system. This feature of the local system has been verified in [19], where local systems were modelled as energy hubs, and an integrated model was established to optimally schedule the regional and local systems. In real-world practice, however, local systems and regional systems are owned and operated by different entities. In general, the RSO can neither control nor obtain information access to consumer-owned devices. Hence, it is impractical to integrate the flexibility of local IDR through centralized optimization. As demonstrated in Fig. 1, local systems are interfaced with the regional system at the property division point (PDP). A viable method is to obtain an external equivalence of each local system and schedule the regional system with an external description. The external characteristics of the IDR of the local multi-energy system are modelled and described explicitly via a novel concept, namely integrated flexibility.

B. Integrated Flexibility

The integrated flexibility is defined as the ability of the local multi-energy system equipped with energy converters to serve its fixed terminal multi-energy loads with adjustable energy inputs through IDR programs. This ability naturally arises from the multi-energy synergy at the local level. The local system "reprocesses" the multi-energy flow imported from the regional system to serve the terminal MED. Owing to the mutual alternatives among different energy carriers and the capacity redundancy of converters, the terminal MED can be satisfied with a variety of combinations of multi-energy inputs.

For instance, one may consider a local system of which the electricity demand is served simultaneously by the utility grid and a local gas-fired combined heat and power (CHP) unit, while the heat load is served only by the CHP unit. Assume that the CHP unit is an extraction condensing unit, of which the electricity-heat ratio is adjustable within a certain range. The local system imports electricity and natural gas from the regional system and converts them into electricity and heat to serve the local demand. Since the terminal MED is fed by different sources, the local system can use different combinations of electricity and natural gas from the utility system to feed a fixed amount of its terminal MED. This feature may bring both economic and environmental benefits to the entire system. When the regional power grid is congested or in a state of emergency, the electricity of the local system can shift from grid-supplied electricity to local CHP-generated electricity, which may help alleviate regional transmission congestion or emergencies. Besides, when the regional renewable generation is in a surplus, the local system can input more electricity from the regional system and reduce its gas input, which is helpful to accommodate renewable generation and reduce emissions from fossil fuels.

To embed the integrated flexibility provided by local systems into the regional system optimization, the capability of the integrated flexibility provision has to be explicitly characterized and submitted to the RSO. In this paper, we define the feasible region of IDR as the allowable range of multi-energy flexibility that a local system can provide to the regional system without violating internal operation constraints and curtailing its terminal energy demand. To illustrate the basic framework of the integrated flexibility provision, the feasible region is modelled in a compact form in this subsection, while detailed models and estimation methods will be elaborated in Section III. Regard each local multi-energy system as an energy hub with multiple inputs and outputs. For the i^{th} local system, let $\boldsymbol{V}^{ls,i}$ denote the vector of its internal energy flows. Let $\boldsymbol{A}_{in}^{ls,i}$ and $\boldsymbol{A}_{out}^{ls,i}$ denote the incidence matrices of the input and output ports to the internal energy flow vector, respectively. Then, the input and output energy flow vectors of the local system can be represented as $\boldsymbol{V}_{in}^{ls,i}=\boldsymbol{A}_{in}^{ls,i}\boldsymbol{V}^{ls,i}$ and $\boldsymbol{V}_{out}^{ls,i}=\boldsymbol{A}_{out}^{ls,i}\boldsymbol{V}^{ls,i}$, respectively. Given the terminal MED $\boldsymbol{D}^{ls,i}$, the operation feasible region of the local system is denoted as $\boldsymbol{\Phi}^i(\boldsymbol{D}^{ls,i})$ and can be represented as the following compact form:

$$\boldsymbol{\Phi}^i(\boldsymbol{D}^{ls,i})=\{\boldsymbol{V}^{ls,i}\big|\,\boldsymbol{g}^{ls,i}(\boldsymbol{V}^{ls,i})\leq\boldsymbol{0},\ \boldsymbol{A}_{out}^{ls,i}\boldsymbol{V}^{ls,i}=\boldsymbol{D}^{ls,i}\} \tag{1}$$

The multi-row equalities $\boldsymbol{g}^{ls,i}(\cdot)\leq\boldsymbol{0}$ represent the operation constraints of the energy hub. A detailed formulation will be derived in Section III.

Mathematically, the feasible region of IDR is then formulated as the projection of the operation feasible region $\boldsymbol{\Phi}^i(\boldsymbol{D}^{ls,i})$ onto the subspace of the input vector space, i.e.,

$$\boldsymbol{\Omega}^i(\boldsymbol{D}^{ls,i})=\{\boldsymbol{V}_{in}^{ls,i}\big|\,\exists\ \boldsymbol{V}^{ls,i}\in\boldsymbol{\Phi}^i(\boldsymbol{D}^{ls,i}),\ \boldsymbol{V}_{in}^{ls,i}=\boldsymbol{A}_{in}^{ls,i}\boldsymbol{V}^{ls,i}\} \tag{2}$$

$\boldsymbol{\Omega}^i(\boldsymbol{D}^{ls,i})$ includes all possible values of the input energy vector that can be converted to meet the terminal MED of the local system without violating any system operation constraints. Embedding the flexibility of local system in the optimal scheduling of regional system will ensure that the scheduling results are executable for the local system.

C. Coordination Scheme

With the explicit representation of the feasible region of IDR, the regional and local multi-energy systems can be optimally coordinated through the following scheme.

1) The RSO makes an optimal schedule of system production in advance, for example, a day-ahead schedule according to its load forecast of each energy node and local system.

2) Each local system estimates its feasible region of IDR based on its forecasting result of the terminal MED, and then provides it to the RSO at certain intervals.

3) According to the contingency type, real-time load, and feasible region of IDR of local systems, the RSO optimally schedules utility-level regional system and determines the multi-energy inputs of local systems.

Let $\boldsymbol{v}^{rs}$ and $\boldsymbol{s}^{rs}$ denote the vector of multi-energy flows and state variables of the regional system, respectively. Let $\boldsymbol{v}_{in}^{rs}$ denote the resource input vector of the regional system. Let $\boldsymbol{V}_{in}^{ls}=\{\boldsymbol{V}_{in}^{ls,1},\boldsymbol{V}_{in}^{ls,2},...,\boldsymbol{V}_{in}^{ls,N_{ls}}\}$, where N_{ls} is the number of local systems. Let $\boldsymbol{v}_{in}^{rs,p}$ and $\boldsymbol{s}^{rs,p}$ denote the resource input and state vectors decided by RSO in the first step, respectively. Let $C^{rs}(\cdot)$ and $\boldsymbol{h}(\cdot)$ denote the cost function and the operation constraints of the regional system, respectively. Then, the optimal scheduling model solved by the RSO can be expressed as:

$$\min_{\boldsymbol{v}^{rs},\boldsymbol{s}^{rs},\boldsymbol{v}_{in}^{rs}} C^{rs}(\boldsymbol{v}_{in}^{rs},\boldsymbol{s}^{rs}) \tag{3}$$

s.t.

$$\boldsymbol{h}(\boldsymbol{v}^{rs},\boldsymbol{s}^{rs},\boldsymbol{v}_{in}^{rs},\boldsymbol{V}_{in}^{ls})\leq \boldsymbol{0} \tag{4}$$

$$\left|\boldsymbol{v}_{in}^{rs}-\boldsymbol{v}_{in}^{rs,p}\right|\leq \boldsymbol{\varepsilon} \tag{5}$$

$$\left|\boldsymbol{s}^{rs}-\boldsymbol{s}^{rs,p}\right|=\boldsymbol{0} \tag{6}$$

Constraints (5) and (6) represent corrective control constraints in which state variables such as the decision of generators to start up or shut down should be fixed while the resource input variables such as the output of generators are allowed to change within a given range $\boldsymbol{\varepsilon}$ under $N-1$ contingency or load fluctuating situation in the real-time scheduling stage of RSO. In this way, the flexible resources of local systems can be considered and dispatched by the RSO, thus reducing contingency impact and potential line investment.

The above coordination scheme can be implemented in a distributed fashion, i.e., the RSO does not have to collect detailed information of all local systems or get control access to local devices. Instead, the RSO only has to obtain the external characteristics of local systems and determine the inputs needed by local systems. Compared with the integrated optimization of the regional and local systems, the proposed coordination scheme is more acceptable in practice, where internal information and control access of local systems are hardly open to the RSO.

In the proposed scheme, the first step is usually applied in a day-ahead way to determine the day-ahead schedule, while the last two steps are used in real-time dispatch where the system operator collects local system information and utilizes the flexibility of local systems. The above three steps can also be coordinated together in a day-ahead way to perform a security-constrained schedule, if all kinds of contingencies are taken into consideration in the third step and the dispatch results of the first step are requested to guarantee a feasible solution under all contingency situations within the adjustment ability of the resource input and local systems.

III. Mathematical Model

A. Feasible Region Model of IDR

Equations (1) and (2) give a compact form of the feasible region of IDR of a local system while its specific derivation depends on the characteristics of the local system, which will be further explained in this subsection.

The local system, which consists of production components and converters of different energy systems, is illustrated by the energy conversion and local security constraints proposed in our previous work [18] as:

$$\boldsymbol{H}_m^{ls,i}\boldsymbol{A}_m^{ls,i}\boldsymbol{V}^{ls,i}=\boldsymbol{0} \tag{7}$$

$$\boldsymbol{Q}_m^{ls,i}\boldsymbol{A}_m^{ls,i}\boldsymbol{V}^{ls,i}\leq \boldsymbol{q}_m^{ls,i} \tag{8}$$

$$\boldsymbol{0}\leq \boldsymbol{V}^{ls,i}\leq \overline{\boldsymbol{V}}^{ls,i} \tag{9}$$

The energy conversion constraint (7) is formulated by the energy conversion matrix $\boldsymbol{H}_m^{ls,i}$, which illustrates the energy conversion efficiency of node m in the i^{th} local system. $\boldsymbol{A}_m^{ls,i}$ represents the coupling matrix of ports of node m and energy flows, whose elements 1 and -1 represent that the port is the sink and source of the branch of energy flow, respectively, and 0 represents that the port is not connected to the branch. Similarly, the security constraint (8) is derived from the operation constraints of local energy converters, including capacity limits, coupled electricity-heat output constraints of the extraction condensing CHP, etc. The coefficient matrix of node m in the i^{th} local system $\boldsymbol{Q}_m^{ls,i}$ and vector $\boldsymbol{q}_m^{ls,i}$ are involved in the expression to form the constraint. The security constraint (9) represents transfer capacity limits $\overline{\boldsymbol{V}}^{ls,i}$ and unidirectionality of energy flows. The specific implication and definition of the abovementioned matrix and model are involved in [20].

From the above constraints, the feasible region of the energy flows of the local system in (1) can be formulated in detail as (10), after which the feasible region of IDR of the local system can be derived through (2).

$$\boldsymbol{\Phi}^i(\boldsymbol{D}^{ls,i})=\{\boldsymbol{V}^{ls,i}\big|(7)\text{-}(9),\boldsymbol{A}_{out}^{ls,i}\boldsymbol{V}^{ls,i}=\boldsymbol{D}^{ls,i}\} \tag{10}$$

B. Network Model

The network model mainly consists of the steady-state operation characteristics of the electricity, gas, and heat systems, including their production, transmission, and consumption processes. The electricity network constraints are similar to those of the unit commitment problem, which are expressed as:

$$\sum_{g\in\mathcal{U}^G}P_{g,t}=\sum_{n\in\mathcal{N}^P}P_{n,t}^L \quad \forall t\in\mathcal{T} \tag{11}$$

$$\sum_{g\in\mathcal{U}^G}(P_{g,\max}-P_{g,t})U_{g,t}\geq SR_t^r \quad \forall t\in\mathcal{T} \tag{12}$$

$$-F_{k,\max}\leq P_{k,t}\leq F_{k,\max} \quad \forall k\in\mathcal{L}^P, t\in\mathcal{T} \tag{13}$$

$$P_{k,t}=\sum_{g\in\mathcal{U}^G}GSDF_{k,N(g)}\cdot P_{gt}-\sum_{n\in\mathcal{N}^P}GSDF_{k,n}\cdot P_{n,t}^L \quad \forall k\in\mathcal{L}^P, t\in\mathcal{T} \tag{14}$$

$$P_{g,\min}U_{g,t}\leq P_{g,t}\leq P_{g,\max}U_{g,t} \quad \forall g\in\mathcal{U}^G, t\in\mathcal{T} \tag{15}$$

$$\left|P_{g,t}-P_{g,t-1}\right|\leq Ramp_g \quad \forall g\in\mathcal{U}^G, t\in\mathcal{T} \tag{16}$$

$$\sum_{i=1}^{t_{g,\min}^{on}}U_{g,t-i}\geq t_{g,\min}^{on}Z_{g,t} \quad \forall g\in\mathcal{U}^G, t\in\mathcal{T} \tag{17}$$

$$\sum_{i=1}^{t_{g,\min}^{off}}U_{g,t-i}\leq t_{g,\min}^{off}(1-Y_{g,t}) \quad \forall g\in\mathcal{U}^G, t\in\mathcal{T} \tag{18}$$

Formula (11) represents the system power balance. Formula (12) shows the system reserve requirement. Formulas (13) and (14) are the network transmission constraints. Formulas (15)-(18) are the unit output and the minimum start-up/shutdown time constraints, which are enforced through 0-1 integer variables $U_{g,t}$, $Y_{g,t}$, and $Z_{g,t}$.

The gas constraints are also based on the steady-state operation characteristics, mainly determined by gas node pressure and the flow through gas wells, pipelines, and compressors, which are modelled as (19)-(23). The time subscript is omitted here, as no temporal coupling exists in the constraints.

$$\sum_{s \in \mathcal{U}_m^{gs}} v_s - \sum_{l \in \mathcal{U}_m^{gl}} L_l - \sum_{n \in \mathcal{N}_m^{gn}} f_{mn} - \sum_{j \in \mathcal{U}_m^{gc}} F_{f,j} = 0 \quad \forall m \in \mathcal{N}^G \tag{19}$$

$$f_{mn} = sgn(\pi_m - \pi_n) C_{mn} \sqrt{\left| \pi_m^2 - \pi_n^2 \right|} \tag{20}$$

$$f_{mn} = sgn(\pi_m - \pi_n) \frac{H_j}{k_{j2} - k_{j1} \left(\dfrac{\max(\pi_m, \pi_n)}{\min(\pi_m, \pi_n)} \right)^{\alpha}} \tag{21}$$

$$F_{f,j} = c_j + b_j H_j + a_j H_j^2 \quad \forall j \in \mathcal{U}^{gc} \tag{22}$$

$$\begin{cases} \pi_{m,\min} \le \pi_m \le \pi_{m,\max} & \forall m \in \mathcal{N}^G \\ v_{s,\min} \le v_s \le v_{s,\max} & \forall s \in \mathcal{U}^{gs} \\ H_{j,\min} \le H_j \le H_{j,\max} & \forall j \in \mathcal{U}^{gc} \end{cases} \tag{23}$$

The above model is a classical gas system model [21]. Formula (19) represents the nodal balance of gas flow. Formulas (20) and (21) are utilized to determine the amount of gas flow through a pipeline or a compressor. Formula (22) derives the loss of gas flow through a compressor. Formula (23) shows the capability or operation range of certain components, including the nodal pressure, gas supply capability, and power of compressors.

The heat constraints are derived from the steady-state physical property between the flow mass and the heat transmission through the heat pipeline [22]. To simplify the problem, we assume that heat transmission is adjusted through the temperature of fluid instead of its flux. Additionally, the time-delay property is ignored in this paper. The heat network model is thus described as (24)-(27), and the time subscript is also omitted here.

$$\begin{cases} \displaystyle\sum_{p \in \mathcal{L}_q^{H,+}} m_p T_{p,out}^{s/b} = T_q^{s/b} \sum_{p \in \mathcal{L}_q^{H,-}} m_p \\ T_{p,in}^{s/b} = T_q^{s/b} \end{cases} \quad \forall p \in \mathcal{L}_q^{H,-}, q \in \mathcal{N}^H \tag{24}$$

$$\begin{cases} T_{p,out}^{s/b} = (T_{p,in}^{s/b} - T_a) \mathrm{e}^{-\frac{\lambda L_p}{c m_p}} + T_a \\ \mathrm{e}^{-\frac{\lambda L_p}{c m_p}} \approx 1 - \dfrac{\lambda L_p}{c m_p} \end{cases} \quad \forall p \in \mathcal{L}^H \tag{25}$$

$$Q_q^{s/l} = c m_p (T_p^s - T_p^b) \quad \forall p \in \mathcal{L}^{Hs/Hl} \cap \mathcal{L}_q^H \tag{26}$$

$$\begin{cases} T_{\min}^s \le T_{p,out}^s \le T_{\max}^s & \forall p \in \mathcal{L}^{H,s} \\ T_{\min}^s \le T_{p,in}^s \le T_{\max}^s & \forall p \in \mathcal{L}^{H,s} \\ T_{\min}^b \le T_{p,out}^b \le T_{\max}^b & \forall p \in \mathcal{L}^{H,b} \\ T_{\min}^b \le T_{p,in}^b \le T_{\max}^b & \forall p \in \mathcal{L}^{H,b} \end{cases} \tag{27}$$

Formula (24) describes the procedure of heat mixing at node q, representing the heat mix balance constraint and the nodal outflow temperature constraint. Formula (25) models the heat loss during the transmission procedure through a pipeline, reflected in the difference between the temperature of the fluid outflow and inflow of the pipeline, which can be further linearized to simplify the calculation. Formula (26) shows the relationship between the heat supply or load and the fluid flux combined with its temperature. The subscripts of the temperature variables in (26) are omitted as the heat loss is assumed to be zero in the pipelines directly connected with the heat supply and load. Formula (27) represents the temperature limit of the network.

The proposed network model adopts a DCOPF-based power system model and neglects the time-delay property of the heat system. Future studies may attempt to present a more elaborate model such as a distribution network model.

C. Coordinated Optimization

Different energy systems are connected through the energy production and consumption processes. The consumption process includes the integrated flexibility provided by the local system, whose model has been introduced in Section III-A. This subsection will mainly introduce the model used in other energy conversion processes.

Formula (28) shows the relationship between the gas input and power output of gas-fired generators, where gas consumption is modelled as a quadratic function of the power output, whose coefficients are represented by af_i, bf_i, and cf_i. The gas contract here is assumed to be a flexible contract which only fixes the gas price in advance.

$$L_{i,t} = (af_i \cdot P_{i,t}^2 + bf_i \cdot P_{i,t} + cf_i) U_{i,t} \quad \forall i \in \mathcal{U}^{GF}, t \in \mathcal{T} \tag{28}$$

Formula (29) shows the relationship between the gas input and heat output of gas-fired generators, where the coefficent C_i^{boiler} reflects the energy conversion efficiency from gas to heat. The cost here is also determined by the cost of gas consumption.

$$Q_{i,t} = C_i^{boiler} L_{i,t} \quad \forall i \in \mathcal{U}^{GB}, t \in \mathcal{T} \tag{29}$$

The above gas costs are determined by the gas price multiplied by gas consumption, as shown in (30). The set $\mathcal{U}^{gl}$ here not only involves the gas load of gas boilers (GBs) and gas-fired generators, but also contains that of local systems.

$$W_{i,t} = L_{i,t} \rho_i \quad \forall i \in \mathcal{U}^{gl}, t \in \mathcal{T} \tag{30}$$

Formula (31) shows the relationship between the power and heat output of CHP units. In this way, we assume that the CHP unit works in the backpressure mode when its power output is in direct proportion to heat output.

$$Q_{i,t} = P_{i,t} C_i^{CHP} \quad \forall i \in \mathcal{U}^{CHP}, t \in \mathcal{T} \tag{31}$$

In a coordinated system, the load in different energy sections is divided into three categories, including fixed load, fluctuating load, and IDR load. The first category is given as a forecast value, and the second category is supposed to be available within a given range, while the third category satisfies the constraint that the electricity, heat, and gas consumption connected to the same SEH vary in a given feasible region determined by its physical characteristics, as stated in Section III-A.

In day-ahead scheduling, for example, given the load forecast information, the complete model to minimize the operation cost of the regional system while satisfying the system load can be written as:

$$\begin{cases} \min Obj = f(v_{in}^P, v_{in}^Q, v_{in}^G) \\ \text{s.t. (2), (10)-(17)} \end{cases} \tag{32}$$

The objective function in (32) is related with the multi-energy input variables of the regional system $v_{in}^P, v_{in}^Q, v_{in}^G$, which can be expanded to the sum of the cost of each energy production process, as shown by (33). Here, $f_i^{CHP}(\cdot)$ and $f_i^{CF}(\cdot)$ represent the quadratic cost functions of coal-fired CHPs and thermal generators, respectively, as the costs of gas-fired CHPs and thermal generators are included in the gas costs.

$$f=\sum_t\left\{\sum_{i\in\mathcal{U}^{gl}}W_{i,t}+\sum_{i\in\mathcal{U}^{CHP}}f_i^{CHP}(P_{i,t},Q_{i,t})U_{i,t}+\sum_{i\in\mathcal{U}^{CF}}f_i^{CF}(P_{i,t})U_{i,t}+\sum_{i\in\mathcal{U}^{G}}(SU_{i,t}+SD_{i,t})\right\} \tag{33}$$

By introducing a large penalty factor of the slack variable of line flow, the impact of the $N-1$ contingency on the violation of transmission capacity constraints can be studied. The slack variables, representing the maximum power flow violation of power transmission lines, will remain zero when no power flow violation occurs. However, if violation is inevitable when the adjustment ability of IDR and generators is insufficient, the slack variable will be exactly the maximum violation value of the line capacity. In this way, the objective function can be rewritten as:

$$f=\sum_t\left\{\sum_{i\in\mathcal{U}^{gl}}W_{i,t}+\sum_{i\in\mathcal{U}^{CHP}}f_i^{CHP}(P_{i,t},Q_{i,t})U_{i,t}+\sum_{i\in\mathcal{U}^{CF}}f_i^{CF}(P_{i,t})U_{i,t}+\sum_{i\in\mathcal{U}^{G}}(SU_{i,t}+SD_{i,t})+\sigma\sum_{k\in\mathcal{L}^P}sl_k\right\} \tag{34}$$

At the same time, the line flow constraint (13) should be rewritten as:

$$-F_{k,\max}-sl_k\le P_{k,t}\le F_{k,\max}+sl_k \quad sl_k\ge 0 \tag{35}$$

In this paper, only tripping contingencies of power system transmission lines and their impact are discussed. Contingency and its impact in other systems may be further studied in the future. The entire model is a mixed-integer nonlinear programming problem, while after applying piecewise linearization in [23] to the gas flow constraints, it can be transformed into a linear model, which can be solved using mainstream optimization solvers.

IV. Case Study

In this section, a multi-energy system containing electricity, gas, and heat systems is proposed, in which different energy sources and local integrated energy conversion models are embedded. The benefits of applying local system flexibility to alleviate the impacts caused by $N-1$ tripping contingencies of power system transmission lines are analyzed based on the case system.

A. System Description

The proposed multi-energy system is based on a modified 24-node IEEE RTS96 power system, together with a 7-node gas system and three independent 4-node heat systems. Its topology is shown in Fig. 2.

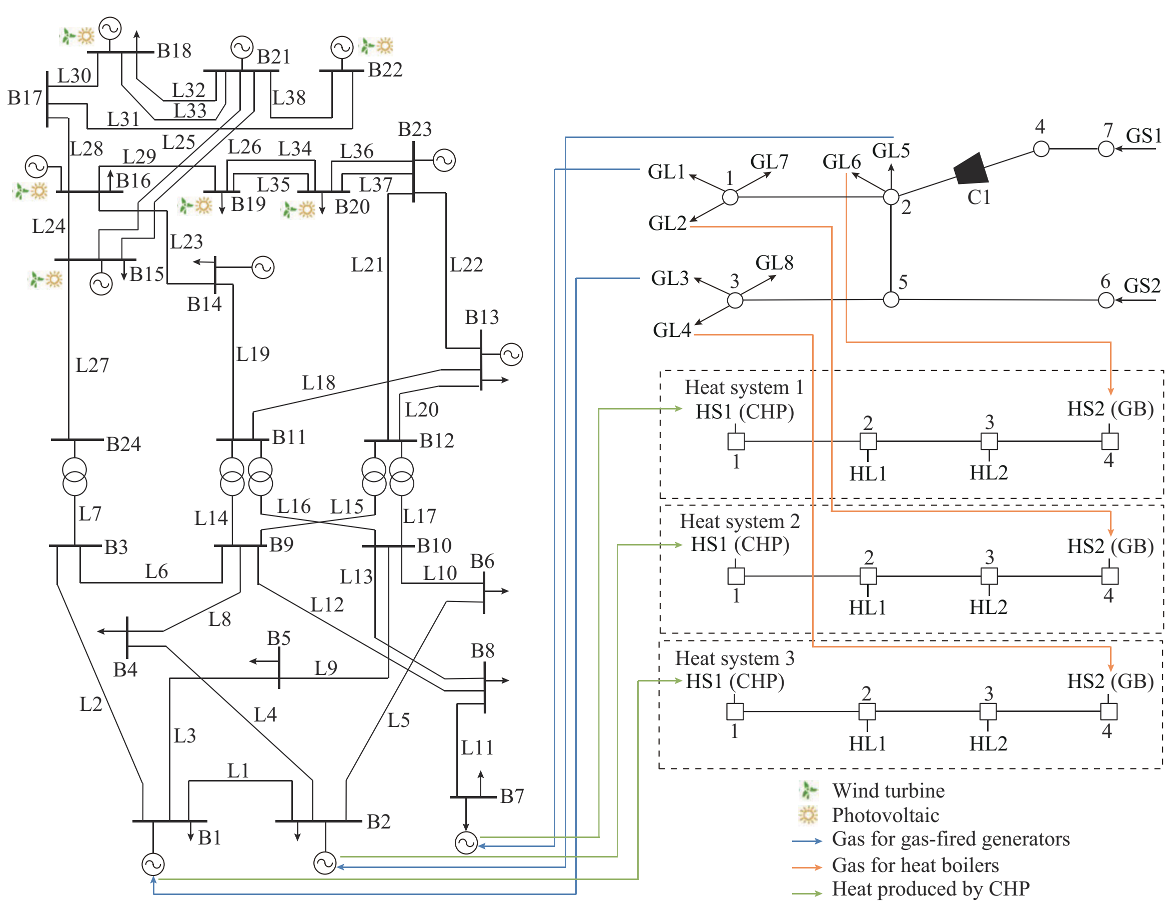

Fig. 2. Topology of proposed multi-energy system.

In the proposed power system, three of the generators are replaced by gas-fired CHP generators, and renewable resources, including wind and solar energy, are added in the top half of the system. The total installed capacities of thermal generators, gas-fired CHPs, and renewable generators are 3153 MW, 252 MW, and 1300 MW, respectively. The load of the power system includes fixed residential load and load connected to the SEH. The 7-node gas system, whose model data can be found in [21], contains 2 gas wells (GS1 and GS2), 5 gas pipelines, and 1 compressor (C1). The total gas production capacity is 11.3 Mcf/h. The load of the gas system includes the fixed residential load (GL7), SEH load (GL8), and consumptions of GBs and gas-fired generators (GL1-GL6). The heat system consists of 2 heat sources (HS1 and HS2), 2 heat loads (HL1 and HL2), and 3 pipelines connecting them. The heat sources are connected with CHP generators and GBs whose heating capacities are 130 MW and 100 MW, respectively, while the heat loads are assumed to be the sum of the fluctuating load within a given range and SEH load. The three SEHs are connected to gas node 3, power buses B4, B5, and B8, and heat node 2 in the three heat systems. Each local SEH contains an electric transformer, a gas-fired CHP, a GB, and an electric heat pump, whose rated capacities are 150 MW, 150 MW, 75 MW, and 30 MW, respectively. The system-wide information of the proposed multi-energy system and the standardized system loads are shown in Table I and Fig. 3, respectively, where the heat production cost is assumed as the cost of the consumed electricity and gas; and 1 kilo-cubic feet of natural gas is assumed to generate 1 MBtu of energy. The standardized load of each energy carrier equals the hourly load divided by its daily maximum load.

TABLE I
SYSTEM-WIDE INFORMATION OF PROPOSED MULTI-ENERGY SYSTEM

System	Total capacity	The maximum load	Production cost
Electricity system	4705 MW	2850 MW	41-128 $/MWh
Gas system	11.3 Mcf/h	6.64 Mcf/h	6.23 $/Mbtu
Heat system	230 MW	155 MW	

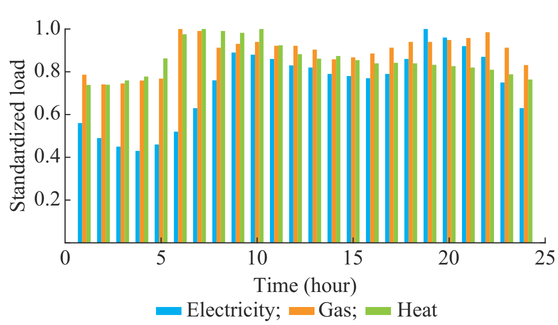

Fig. 3. Standardized system loads.

The case study is formed on a daily basis, while the time interval is set to be one hour. The full optimization problem, as (32) states, is a mixed-integer nonlinear programming problem that can be reformulated into a mixed-integer linear programming (MILP) problem by adopting piecewise linearization methods, as shown in Appendix A. The simplified MILP problem is modelled by GAMS 24.3 using Cplex 12.6 as the solver on a Thinkpad T490 laptop.

B. Illustration of Feasible Region of IDR

The feasible regions of IDR of a local SEH at certain time intervals are shown in Fig. 4. The feasible region reflects the ability of local system to change its load components as the inputs of SEH can be an arbitrary vector within the region to reduce the real-time cost of system or respond to the system order to increase its security margin. For example, the operation point of the IDR can move from an interior point to its border to reduce certain loads when certain equipment is in outage in any energy system.

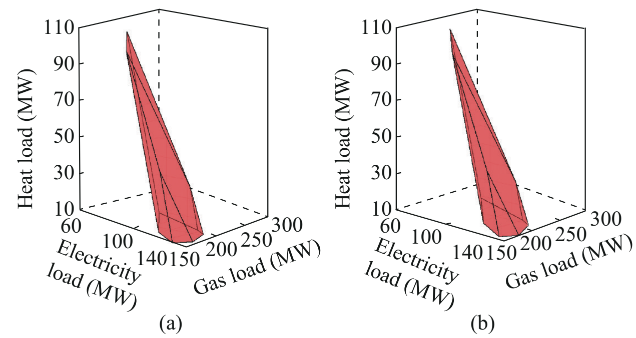

Fig. 4. Feasible regions of IDR of a local SEH. (a) At time interval 9. (b) At time interval 19.

C. Effectiveness of Coordination Framework

In this subsection, 3 scenarios are considered: S1, normal operation without IDR; S2, operation during $N-1$ contingency without IDR; and S3, operation during $N-1$ contingency with IDR. By comparing the slack variable of line capacity and introducing a large penalty term in the objective function, the effectiveness of IDR in alleviating flow violation caused by transmission line tripping is illustrated. The system optimization procedure during line tripping contingencies is similar to that of the methods used in corrective control, in which the start-up and shut-down decisions of the units are fixed to the result of the day-ahead unit commitment in S1, but the power outputs are allowed to change within a given range.

Taking a single line tripping condition as an example, assume that line 27 from node 15 to node 24 is in outage during a whole day. Then, the day-ahead operation optimization of the proposed multi-energy system in three scenarios is performed. The result indicates that the line tripping contingency will make the system infeasible during certain time intervals in S2 and S3 due to the lack of power transmission capacity, and the power flows of certain transmission lines in S2 and S3 is demonstrated in Fig. 5.

From Fig. 5, the power flows of lines 6 and 10 in S2 will exceed the lower bound (−100 MW) in the 9th hour, 18th hour, and 19th hour, while the power flow constraints during these hours are all redundant in S1, which implies that line tripping contingency increases the load rate of lines 6 and 10 and makes the line exceed its maximum capacity

(100 MW), thus making the whole system infeasible in S2. However, the violation capacity of power transmission constraints is greatly reduced in S3 when IDR is considered, as only the power flow of line 6 in the 19th hour exceeds its limit by 12.3 MW compared with the 31.1 MW in S2 due to the load adjustment of the power system.

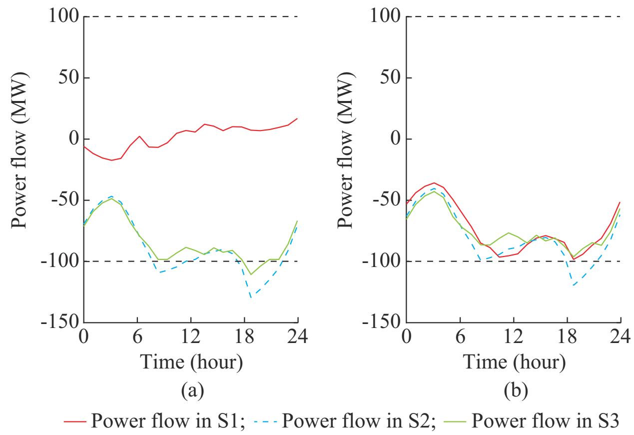

Fig. 5. Power flows of lines 6 and 10 in S1-S3 when line 27 is tripping. (a) Line 6. (b) Line 10.

The total energy load of the local systems participating in IDR is shown in Fig. 6, from which the shedding of electricity load can be observed during these time intervals in S3 compared with the electricity load in S2. More specifically, the local systems use more gas and heat instead of electricity to satisfy the terminal energy requirement, thus providing more feasibility and a greater security margin for power system during power transmission contingencies. If the LTE/STE of the transmission line is considered in the coordination operation procedure, the adoption of IDR can also reduce the requirement of LTE/STE, thus making the whole system safer.

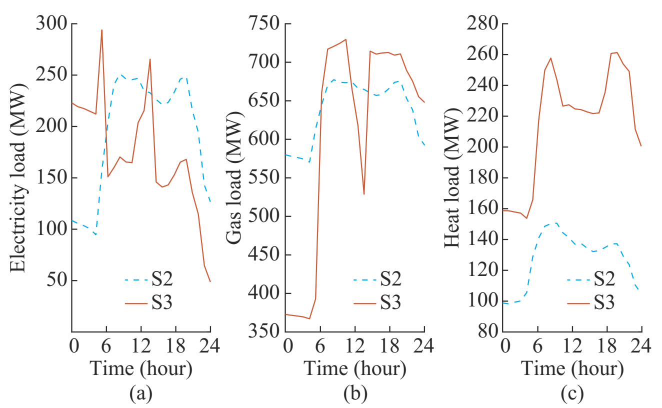

Fig. 6. Total energy load of local systems participating in IDR. (a) Electricity load. (b) Gas load. (c) Heat load.

To be more specific, the system-wide results under the tripping condition of each line, including the feasibility with and without IDR and the total cost with and without IDR, are shown in Table II, where 0 represents the system is infeasible while 1 represents the system is feasible; and the tripping condition of line 11 is ignored as it will cause a "power island". Among all 37 tripping conditions of lines, the adoption of IDR can prevent the infeasibility that line tripping may bring about under 21 tripping conditions. Under 8 tripping conditions, the entire system is feasible in both S2 and S3, where IDR can further reduce the total cost of the system by making terminal loads more rational according to the energy production or transmission situation. For example, the IDR can help to consume renewable energy when there is excessive wind output. Under other conditions such as the abovementioned tripping condition of line 27, taking IDR into consideration can reduce transmission line capacity violations.

TABLE II
SYSTEM-WIDE RESULTS UNDER TRIPPING CONDITON OF EACH LINE

No. of line under tripping condition	Feasibility without IDR	Feasibility with IDR	Total cost without IDR (10^6 \$)	Total cost with IDR (10^6 \$)
5, 7, 9, 16-18, 23, 27	0	0		
4	1	1	2.705	2.667
6	1	1	2.706	2.667
24	1	1	2.708	2.669
28	1	1	2.705	2.666
30	1	1	2.705	2.666
31	1	1	2.714	2.677
32	1	1	2.705	2.667
33	1	1	2.705	2.667
Others	0	1		

After a single-line tripping case, all possible line tripping conditions are studied together, among which the maximum and minimum values of the power flow of each line in each time interval are derived from the optimization results to show the power transmission feasibility change caused by IDRs. Then, the decrease in the maximum slack required by each line through S2 to S3 can also provide a way to quantify the benefits of IDRs in terms of system security. The comparison of the extreme power flows of lines 12 and 13 in S2 and S3 is given in Fig. 7.

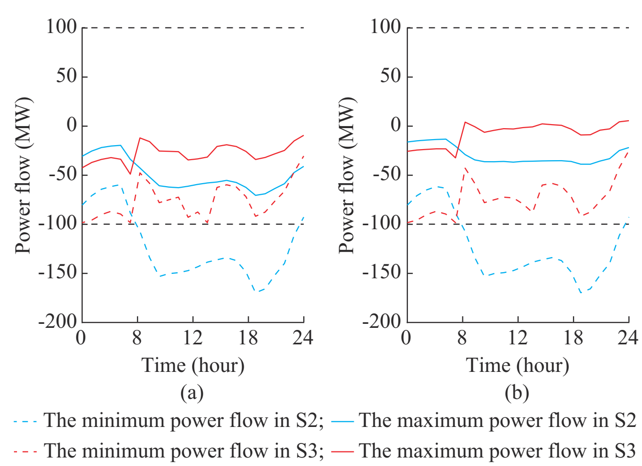

Fig. 7. Extreme power flows of lines 12 and 13 in S2 and S3. (a) Line 12. (b) Line 13.

It can be observed in Fig. 7 that from the 7th hour to the 23rd hour, the extreme power flows of lines 12 and 13 both exceed the lower bound (–100 MW) in S2. However, by adopting IDR instead of the fixed load, the violation capacities of these transmission lines can be reduced from about 71.4 MW to zero, and thus the power flow violation is eliminated, which means that the flexibility provided by IDR contributes to the secure operation of these lines during any $N-1$ contingency.

Table III presents the overall power flow violation condition in S2 and S3 during potential $N-1$ contingency of transmission lines, where the average value is calculated based on the value of violated lines under each condition. The adoption of IDR reduces the number of transmission lines suffering potential violations from 15 to 8, and reduces the total violated time intervals of lines from 141 to 44. Besides, the maximum and average power flow violation capacities also greatly decrease with the adoption of IDR.

TABLE III
OVERALL POWER FLOW VIOLATION CONDITION IN S2 AND S3 DURING POTENTIAL $N-1$ CONTINGENCY OF TRANSMISSION LINES

Parameter	S2	S3
Number of line violations	15	8
Total violated time interval of lines	141	44
The maximum power flow violation capacity (MW)	108.29	45.09
Average power flow violation capacity (MW)	52.29	24.47
The maximum power flow violation rate (%)	72.64	38.33
Average power flow violation rate (%)	31.23	16.41

V. CONCLUSION

To quantify the flexibility of local energy systems and its effect on system operation during contingencies, this paper first proposes a feasible region model of IDR to depict the energy consumption and conversion process of a local system and derive the flexibility of its energy input. The feasible region derived can be embedded into the system scheduling process without detailed information of local system equipment to ensure privacy. A centralized coordination scheme and the optimization model of the entire system are then proposed, based on which the impact of multi-energy flexibility on the power system security margin, in particular, the $N-1$ power system line tripping security, is further studied. Through a multi-energy case system, it demonstrates that the proposed scheme involving IDR of local systems can enhance the power system reliability towards $N-1$ transmission line tripping contingencies. The proposed scheme can be further extended and applied to other energy systems in multi-energy systems to assess their stability in the presence of multiple contingencies.

APPENDIX A

For nonlinear expression $h(x)$ and $x_1 < x_2 < ... < x_n$ in its domain, the linearized process can be stated as (A1) - (A4), where δ_i is a continuous variable and y_i is a binary variable [23].

$$h(x) \approx h(x_1) + \sum_{i=1}^{n-1} (h(x_{i+1}) - h(x_i))\delta_i \tag{A1}$$

$$x = x_1 + \sum_{i=1}^{n-1} (x_{i+1} - x_i)\delta_i \tag{A2}$$

$$\begin{cases} \delta_{i+1} \le y_i \\ y_i \le \delta_i \end{cases} \quad i = 1, 2, ..., n-1 \tag{A3}$$

$$0 \le \delta_i \le 1 \quad i = 1, 2, ..., n \tag{A4}$$

The nonlinear constraints in this paper mainly consist of the following three constraints: the gas consumption constraints of gas-fired generators, gas transmission line constraints, and gas compressor constraints. In the gas consumption equation (28), the quadratic component can be linearized through (A1) - (A4) by letting $h(x)$ denote the square function and x denote the power output.

In the gas flow constraint (20), we assume that for each pipeline, the flow direction is previously determined to eliminate the absolute value. It can also be addressed by introducing a binary variable to compare the pressure of the two ports. If we assume that $\pi_m > \pi_n$, the gas flow constraints can be linearized as (A5) and (A6) with (A3) and (A4) by using the square of pressure as the independent variable and letting $h(\cdot)$ represent the square root calculation and x_1 equal 0.

$$f_{mn} \approx C_{mn} \left(\sum_{i=1}^{n-1} (\sqrt{x_{i+1}} - \sqrt{x_i})\delta_i \right) \tag{A5}$$

$$\pi_m^2 - \pi_n^2 = \sum_{i=1}^{n-1} (x_{i+1} - x_i)\delta_i \tag{A6}$$

In the compressor gas flow constraint (21), we use a step function to estimate the compression ratio π_m/π_n. Additionally, we apply the same assumption in the gas flow equation and use the square of pressure as the independent variable. The estimation is shown as (A7), where R_i represents a series of estimated values in the allowed range, y_i represents a binary variable to choose a R_i as the square of the ratio.

$$\begin{cases} \pi_m^2/\pi_n^2 = \sum_{i=1}^{n} R_i y_i \\ \sum_{i=1}^{n} y_i = 1 \end{cases} \tag{A7}$$

Let parameter $Con_i = 1/(k_{j2} - k_{j1} R_i^{\alpha/2})$. Then the compressor flow can be expressed as:

$$f_{mn} = \sum_{i=1}^{n} Con_i (y_i H_j) \tag{A8}$$

The above expression involves the product of a binary variable and a continuous variable and still requires some skills to be transformed into a linear expression. Let $G = YX$, which represents the value of the product of a binary variable Y and a continuous variable X. By introducing a large parameter M, it can be expressed in a linear form as:

$$-MY \le G \le MY \tag{A9}$$

$$-M(1-Y) \le X - G \le M(1-Y) \tag{A10}$$

References

[1] B. Stott, O. Alsac, and A. J. Monticelli, "Security analysis and optimization," *Proceedings of the IEEE*, vol. 75, no. 12, pp. 1623-1644, Dec. 1987.

[2] K. W. Hedman, M. C. Ferris, R. P. O'Neill *et al*., "Co-optimization of generation unit commitment and transmission switching with $N-1$ reliability," *IEEE Transactions on Power Systems*, vol. 25, no. 2, pp. 1052-1063, May 2010.

[3] D. A. Tejada-Arango, P. Sánchez-Martın, and A. Ramos, "Security constrained unit commitment using line outage distribution factors," *IEEE Transactions on Power Systems*, vol. 33, no. 1, pp. 329-337, Jan. 2018.

[4] Y. Wang, Q. Xia, M. Zhu *et al*., "Optimal corrective security constrained unit commitment model and algorithm," *Automation of Electric Power Systems*, vol. 35, no. 9, pp. 19-24, May 2011.

[5] S. Maslennikov and E. Litvinov, "Adaptive emergency transmission rates in power system and market operation," *IEEE Transactions on Power Systems*, vol. 24, no. 2, pp. 923-929, May 2009.

[6] Y. Fu, M. Shahidehpour, and Z. Li, "AC contingency dispatch based on security-constrained unit commitment," *IEEE Transactions on Power Systems*, vol. 21, no. 2, pp. 897-908, May 2006.

[7] C.-L. Su and D. Kirschen, "Quantifying the effect of demand response on electricity markets," *IEEE Transactions on Power Systems*, vol. 24, no. 3, pp. 1199-1207, Aug. 2009.

[8] Y. Wang, I. R. Pordanjani, and W. Xu, "An event-driven demand response scheme for power system security enhancement," *IEEE Transactions on Smart Grid*, vol. 2, no. 1, pp. 23-29, Mar. 2011.

[9] J. Wang, H. Zhong, Z. Ma *et al*., "Review and prospect of integrated demand response in the multi-energy system," *Applied Energy*, vol. 202, pp. 772-782, Jul. 2017.

[10] Z. Chen, Y. Sun, X. Ai *et al*., "Integrated demand response characteristics of industrial park: a review," *Journal of Modern Power Systems and Clean Energy*, vol. 8, no. 1, pp. 15-26, Jan. 2020.

[11] S. Zheng, Y. Sun, B. Li *et al*., "Incentive-based integrated demand response for multiple energy carriers considering behavioral coupling effect of consumers," *IEEE Transactions on Smart Grid*, vol. 11, no. 4, pp. 3231-3245, Jul. 2020.

[12] S. Bahrami and A. Sheikhi, "From demand response in smart grid toward integrated demand response in smart energy hub," *IEEE Transactions on Smart Grid*, vol. 7, no. 2, pp. 650-658, Mar. 2016.

[13] C. Shao, Y. Ding, P. Siano *et al*., "A framework for incorporating demand response of smart buildings into the integrated heat and electricity energy system," *IEEE Transactions on Industrial Electronics*, vol. 66, no. 2, pp. 1465-1475, Feb. 2019.

[14] F. Dababneh and L. Li, "Integrated electricity and natural gas demand response for manufacturers in the smart grid," *IEEE Transactions on Smart Grid*, vol. 10, no. 4, pp. 4164-4174, Jul. 2019.

[15] P. Liu, T. Ding, Z. Zou *et al*., "Integrated demand response for a load serving entity in multi-energy market considering network constraints," *Applied Energy*, vol. 250, pp. 512-529, May 2019.

[16] D. Chen, C. Wan, Y. Song *et al*., "$N-1$ security-constrained coordinated scheduling of integrated electricity and natural gas system considering gas dynamics and wind power uncertainty," *IET Renewable Power Generation*, vol. 15, no. 7, pp. 1408-1421, Mar. 2021.

[17] H. Chen, J. Shao, T. Jang *et al*., "Static $N-1$ security analysis for integrated energy system based on decoupled multi-energy flow calculation method," *Automation of Electric Power Systems*, vol. 43, no. 17, pp. 20-35, Jul. 2019.

[18] Z. Tan, H. Zhong, Q. Xia *et al*., "Exploiting integrated flexibility from a local smart energy hub," in *Proceedings of 2020 IEEE PES General Meeting*, Montreal, Canada, Aug. 2020, pp. 1-5.

[19] M. Geidl and G. Andersson, "Optimal power flow of multiple energy carriers," *IEEE Transactions on Power Systems*, vol. 22, no. 1, pp. 145-155, Feb. 2007.

[20] Y. Wang, N. Zhang, C. Kang *et al*., "Standardized matrix modeling of multiple energy systems," *IEEE Transactions on Smart Grid*, vol. 10, no. 1, pp. 257-270, Jan. 2019.

[21] C. Liu, M. Shahidehpour, Y. Fu *et al*., "Security-constrained unit commitment with natural gas transmission constraints," *IEEE Transactions on Power Systems*, vol. 24, no. 3, pp. 1523-1536, Aug. 2009.

[22] M. Pirouti, "Modelling and analysis of a district heating network," Ph.D. dissertation, Cardiff University, Cardiff, 2013.

[23] C. M. Correa-Posada and P. Sánchez-Martın. (2014, Jun.). Gas network optimization: a comparison of piecewise linear models. [Online]. Available: http://www. optimization-online. org/DB_FILE/2014/10/4580. pdf

Tong Cheng received the B.S. degree in electrical engineering from Tsinghua University, Beijing, China, in 2020. He is currently working toward the Ph.D. degree in electrical engineering at Tsinghua University. His research interests include power system operation and multi-energy systems.

Zhenfei Tan received the B.S. degree in electrical engineering from Tsinghua University, Beijing, China, in 2017. He is currently pursuing the Ph.D. degree in electrical engineering with Tsinghua University. He serves as the Vice-chair of the IEEE PES Tsinghua Student Branch Chapter since 2020. He was a recipient of the "Best-of-the-Best" Conference Paper Award in the IEEE PES General Meeting in 2020. His research interests include distributed and coordinated optimization of power systems.

Haiwang Zhong received the B.S. and Ph.D. degrees in electrical engineering from Tsinghua University, Beijing, China, where he is currently an Associate Professor with the Department of Electrical Engineering. He was a recipient of the ProSPER.Net Young Scientist Award in 2014, the Outstanding Ph. D. Graduate and Outstanding Post-doctor of Tsinghua University. He serves as the Editor for the International Transactions on Electrical Energy Systems, an Associate Editor for the CSEE Journal of Power and Energy Systems. He currently serves as the Chair of the Demand Response Working Group under the IEEE PES Power System Operations, Planning and Economics Committee, the Secretary of the IEEE PES SBLC Architecture Subcommittee, and the Secretary of CIGRE D2.53 Working Group on Technology and Applications of Internet of Things in Power Systems. His research interests include smart grids, power system operations, electricity markets, and demand response.